Laboratory and numerical investigation of saline intrusion in fractured coastal aquifers

Etsias, G., Hamill, G. A., Campbell, D., Straney, R., Benner, E. M., Aguila, J. F., McDonnell, M. C., Ahmed, A. A., & Flynn, R. (2021). Laboratory and numerical investigation of saline intrusion in fractured coastal aquifers. *Advances in Water Resources*, *149*, Article 103866. https://doi.org/10.1016/j.advwatres.2021.103866

Published in:
Advances in Water Resources

Document Version:
Peer reviewed version

Laboratory and numerical investigation of saline intrusion in fractured coastal aquifers

Georgios Etsias[a,*], Gerard A. Hamill[a], Daniel Campbell[a], Ryan Straney[a], Eric M. Benner[a], Jesus F. Águila[a], Mark C. McDonnell[a], Ashraf A. Ahmed[b], and Raymond Flynn[a]

[a] School of Natural and Built Environment, Queen's University Belfast, Belfast, U.K.

[b] College of Engineering, Design and Physical Sciences, Brunel University, London, U.K.

Corresponding author: Georgios Etsias (G.Etsias@qub.ac.uk)

Highlights

- Saline intrusion in laboratory fractured aquifers was studied for the first time
- The closer the horizontal fractures were to the sea the larger the saline wedge was
- Fracture depth determines the extend of saline intrusion in the vertical direction
- Vertical fractures lead to a significant increase in the width of the mixing zone

Abstract

Laboratory scale experiments and numerical modelling were employed in this study to investigate saltwater intrusion in fractured aquifers. Saline intrusion was initiated in one homogeneous and six fractured experimental aquifers containing individual discontinuities of varying length and orientation. Automated image processing enabled high precision quantification of three intrusion variables, the toe length of the saline wedge, the width of the mixing zone and the aquifer fraction occupied by saltwater. A dual porosity model was successfully utilized to recreate the experimental data and expand the study's findings through rigorous sensitivity analysis. The presence of fractures significantly impacted all three intrusion variables under consideration. The length of intrusion was negatively correlated to the horizontal fracture's distance from the systems' seaward boundary. It was demonstrated that for the same fractured aquifer, the presence of a discontinuity can either limit or augment saline intrusion, depending on the applied hydraulic gradient. For gradients steeper than a critical head difference, at which the toe length was the same for both the fractured and the equivalent homogeneous aquifer, intrusion was suppressed further seaward, while for milder ones it intensified. The distance of horizontal fracture from the aquifer's base determined the extend of intrusion in the vertical direction. In general, the longer the discontinuities were, the more significant their impact on groundwater dynamics. In the case of vertical factures, whenever the saline wedges reached their position, the discontinuities contributed significantly in the widening of the mixing zone, while having limited effect on the other two intrusion characteristics. In aquifers with discontinuities adjacent to their side boundaries, a distinct distribution of saltwater concentration was identified, distinguishing them from the rest of the aquifers.

Keywords:

Saline intrusion, Fractures, Sandbox experiments, SUTRA, Dual-porosity model

1. Introduction

One fourth of the global population depends on freshwater pumped from fractured aquifers (Ford and Williams, 2007), leading to a significant effort to map them and study their hydrogeological characteristics (Bakalowicz et al., 2007; Custodio, 2009; Chen et al., 2017; Montiel et al., 2018). The expected increase in average water consumption, alongside sea level rise due to global warming, is anticipated to intensify saltwater intrusion (SWI) in coastal aquifers. Since fractured systems are more vulnerable to saltwater intrusion than other aquifer types (Arthur et al., 2007), understanding the physical mechanisms governing this phenomenon is of utmost importance. Saline intrusion has been studied in fractured aquifers on multiple locations worldwide, including Canada (Allen et al., 2003), France (Arfib and Charlier, 2016), Greece (Arfib and Marsily, 2004), Ireland (Perriquet et al., 2014), Italy (Masciopinto, 2006), Korea (Lim et al., 2013), the United Kingdom (MacAllister et al., 2018) and the United States (Xu et al., 2016).

Numerical modelling is a long established tool for simulating groundwater flow in real world systems. The numerical approaches employed in the simulation of fractured porous media can be grouped into two categories, implicit and explicit fracture representation models (Sebben et al., 2015; Berre et al., 2018). Implicit fracture representation approaches include single continuum or equivalent porous medium (EPM) models and dual porosity models (DPM). EPM models (Scalnon et al., 2003; Giudici et al., 2012) are single continuum models in which the fractures are represented by adapting the permeability of the porous medium, according to the characteristics of the existing fractures. Dual porosity models (Larsbo and Jarvis, 2005; Fahs et al., 2014) consist of two continua; the matrix, which represents the porous medium and the fracture, which usually has much higher porosity and permeability values. Explicit fracture representation approaches include discrete fracture matrix (DFM) and discrete fracture network (DFN) models. In DFM models the fluid is located in the explicitly represented fractures and the surrounding porous medium alike. DFM models preserve some fractures, while the rest are upscaled and replaced by averaged porous medium quantities. Two dimensional DFM models incorporate fractures as 2-dimensional elements (Jaffré et al. 2005; Angot et al. 2009; Flemisch et al. 2017; Koohbor et al. 2020). DFN models explicitly represent the majority of discontinuities present in a fractured aquifer, and fluid flow occurs mainly within the fracture network. Two-dimensional DFN models represent the geometrical properties of each individual fracture, incorporating them, as 1-dimensional line boundaries between elements (Quinn et al., 2006; Papadopoulou et al., 2008; Hirthe and Graf, 2015; Sebben and Werner, 2016; Ren et al., 2017). Similarly, in 3-d DFN models, fractures are expressed as 2-dimensional planes. The application of each method is associated with specific benefits and limitations (Samardzioska and Popov, 2005; Blessent et al., 2013). EPM approaches are characterized by low levels of computational and model complexity, coming at the cost of oversimplification, that results in inability to represent groundwater flow dynamics in more complex problems. Dual porosity models are generally more successful in simulating the impact of fractures on groundwater flow, to do so though, they introduce different parameters, such as hydraulic conductivity inside the discontinuities and exchange rate coefficients between the matrix and fractures, which are difficult to determine accurately. By contrast, DFM and DFN models are computationally intensive, while the explicit mapping of discontinuities in real-world aquifers is oftentimes problematic.

EPM models are prevalent in regional level studies of SWI in fractured coastal aquifers (Nocchi and Salleolini, 2013; Romanazzi et al., 2015; De Filippis et al., 2016; Steiakakis et al., 2016; Zhao et al., 2016). Dual porosity modelling is more commonly utilized to simulate saline intrusion in aquifers with existing conduit networks, this bigger discontinuity size permits a more precise determination of the network's position inside the aquifers. In the majority of these investigations, flow is considered Darcian both in the porous medium and in the fractures (Xu et al., 2018; Feo et al., 2019; Kreyns et al., 2020). Nevertheless, multiple numerical approaches have been proposed to incorporate turbulent

flow inside the conduits (Arfib and Marsily, 2004; Xu and Hu, 2017; Xu et al., 2019;). Sebben et al. (2015) and Mozafari et al. (2018) simulated a variation of the well-known Henry problem in 2-dimensional aquifers with well-defined networks of individual fractures using DFN modelling. Koohbor et al. (2019) quantified the impact that the uncertainty associated with the position and density of fractures, in discrete fracture networks, has on the simulated saline intrusion dynamics. Both Dokou and Karantzas (2012) and Khadra and Stuyfzand (2018) created hybrid models combining the EPM and DFN approaches in order to optimize SWI simulation in karst systems.

Experimental sandbox setups have been used successfully over the years to investigate saline intrusion in homogeneous (Robinson et al., 2016, Li et al., 2018; Takahasi et al., 2018; Armanuos et al., 2019) and heterogeneous aquifers (Konz et al., 2008; Vithanage et al., 2012; Dose et al, 2014; Liu et al., 2013; Mehdizadeh et al., 2014;). Multiple studies have indicated the significant impact of heterogeneity on SWI dynamics (Abdulhalik and Ahmed, 2017a, b; Houben et al., 2017). Nevertheless, saline intrusion in fractured aquifers has never been studied on a sandbox setup. Laboratory investigations of solute transport in fractured systems have been conducted by Li (2004) and Faulkner et al. (2009). In both studies, glass beads were utilized to recreate the porous medium. In the first investigation, the aquifer had a central vertical conduit running from top to bottom, while in the second study a single horizontal channel was present at the aquifer's lower boundary.

The current study employed sandbox experiments coupled with numerical modelling to study saline intrusion in fractured coastal systems. To the best of the authors' knowledge, this is the first time that SWI in fractured aquifers has been methodically investigated on a laboratory scale. Head induced saline intrusion was initiated across six fractured aquifers, with the experimental data obtained being benchmarked against measurements done on a homogeneous system. The study quantified the impact that the position, size and orientation of individual fractures have on the standard saltwater intrusion characteristics of toe length (TL) of the intruding wedge and the width of the mixing zone (WMZ). Unlike in previous investigations, these intrusion variables were measured with high accuracy, utilizing advanced image analysis techniques (Robison et al., 2015; Etsias et al., 2020 a). The laboratory data were successfully recreated using numerical simulations so that the sandbox measurements were supplemented by an in-depth sensitivity analysis, further expanding the conclusions derived by the experimental observations. This study constitutes a contribution towards outlining the basic mechanisms of SWI in fractured porous media, while its results could assist in the successful management and protection of real-world coastal fractured aquifers.

2. Experimental setup and its correlation with real world fractured aquifers

The sandbox apparatus depicted in Figure 1a was employed in deriving the experimental data of this study. It comprised two cylindrical tanks and a thin central viewing chamber of dimensions 0.38 m × 0.15 m × 0.01 m. Red food colouring (E129 Allura Red AC Granular)was mixed with saltwater at a concentration of 0.15 g/L. The density of the dyed saltwater was equal to 1025 kg/m^3. Transparent general-purpose glass beads with a diameter of 1090 μm, supplied by Whitehouse Scientific®, were siphoned into the viewing chamber to recreate the porous medium of the aquifer. Freshwater was constantly introduced at the bottom of the left chamber, while the right cylinder was filled with dyed saltwater. The water level at each side chamber was regulated using two adjustable height outflow outlets (Figure 1b) placed at the top of the side tanks, while it was constantly monitored by two ultrasonic sensors (Figure 1c) with an accuracy of 0.2 mm. Two laser-cut mesh screens were utilized to secure the glass beads inside the central chamber. Experimental investigations were performed in a dark room; the necessary illumination was provided by two Camtree® 600 LED panels. A Nikon D850 Digital SLR Camera recorded the experimental images at five-minute intervals. The laboratory apparatus was presented in detail by Robinson et al. (2015).

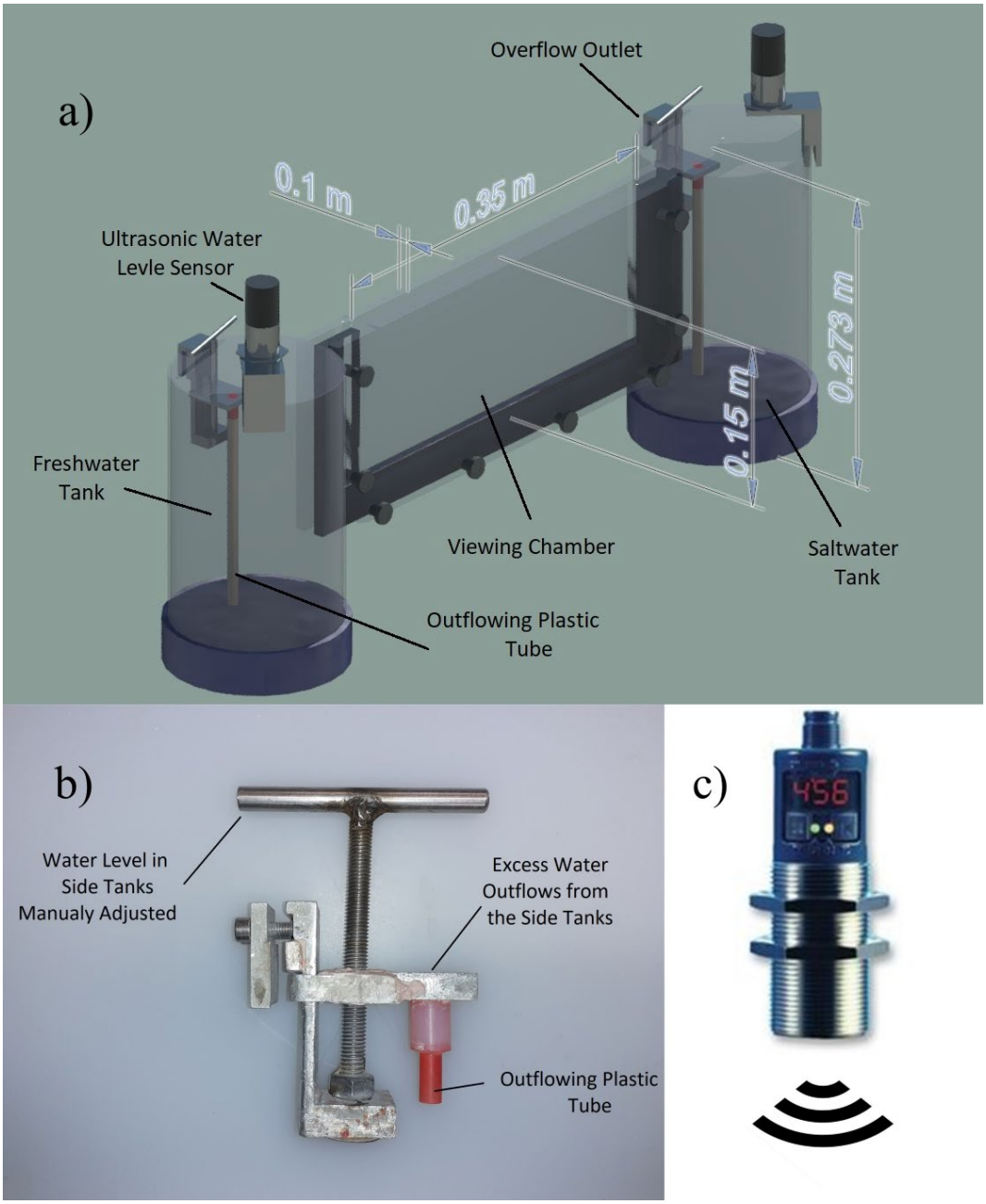

Figure 1: a) 3-dimensional representation of the utilized experimental setup alongside photos of the b) adjustable overflow outlets and c) ultrasonic sensors

Stainless steel mesh screens with 1 mm openings were used to recreate the aquifer fractures. The mesh was manually moulded around a steel rod with an 8 mm diameter. Three hollow mesh cylinders with lengths of 35 cm, 15 cm and 10 cm were created (Figure 2). These structures were placed at pre-determined positions inside the sandbox's viewing chamber, recreating six unique laboratory fractured aquifers (Figure 3). In four cases, the fractures were horizontally oriented, while in the remaining two they were vertical in orientation. In the horizontally fractured aquifers, the cylindrical mesh was placed at the middle of the viewing chamber's height. The first aquifer included the longer fracture (35 cm), crossing most of the porous medium, while in the remaining three test configurations the 15 cm long cylinder was located centrally on the test area mid-point and at the left and right aquifer boundaries respectively. In the vertically fractured test cases, the 10 cm long fracture was placed at the test mid-point and at a distance of 10 cm from the right boundary of the aquifer. In the

interests of clarity, the laboratory aquifers will henceforth be referred to according to their corresponding fracture position: horizontal-long (Figure 3b), horizontal-middle (Figure 3c), horizontal-left (Figure 3d), horizontal-right (Figure 3e), vertical-middle (Figure 3f) and vertical-right (Figure 3g). Testing was also conducted on a homogeneous aquifer, without any fractures, that served as a benchmark case for this investigation (Figure 3a).

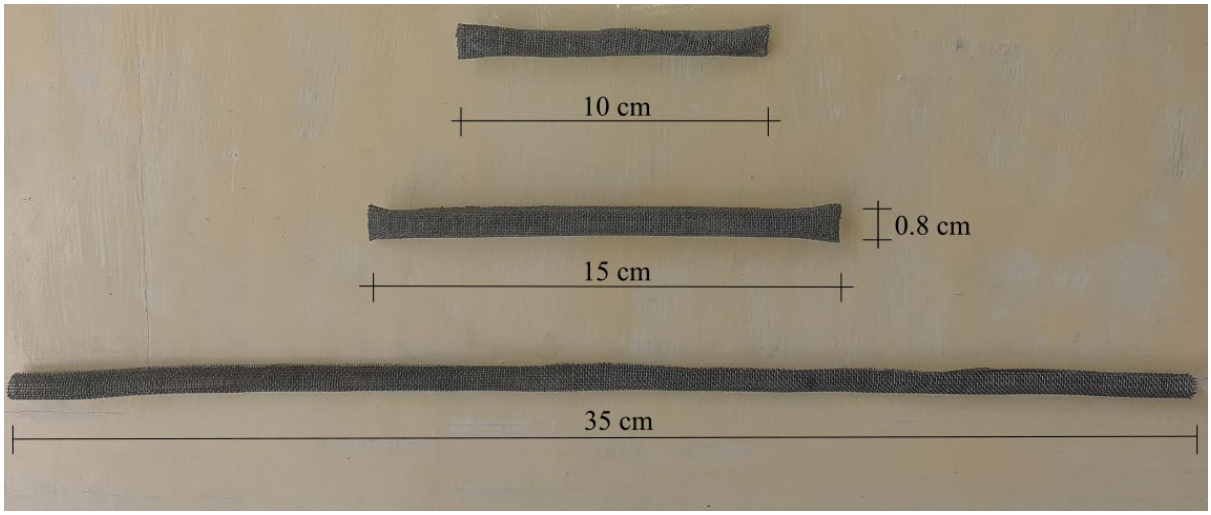

Figure 2: The three hollow mesh cylinders employed to recreate the aquifer fractures during experimental measurements

This is the first ever laboratory study of saltwater intrusion in fractured aquifers. In the absence of any similar investigations, sandbox studies of SWI, alongside fieldwork investigations of saline intrusion in real world fractured hydrological systems, were employed to validate the suitability of the experimental setup in the approximation of fractured aquifers. Glass beads of comparable size have been utilized in multiple laboratory studies of saline intrusion. Zhang et al. (2001 and 2002) used glass beads with a diameter of 725 μm, Goswami and Clement (2007) and Chang and Clement (2013) employed 1.1 mm wide glass spheres, while Konz et al. (2009) studied SWI in heterogeneous aquifers using glass beads of sizes varying between 0.6 mm and 2.2 mm. An intrinsic flow test on the experimental domain allowed calculation of the permeability of the porous media using Darcy's law. Permeability and porosity were equal to 1.83×10^{-9} m^2 and 0.385, respectively. These results agreed with the values reported by Robinson et al. (2015, 2016) for the same laboratory apparatus. Glass beads of similar size have been utilised by Abdelgawad et al. (2017) and Abdoulhalik and Ahmed (2017a, b) in experimental investigations of saltwater upconing.

The permeability measured in the laboratory porous medium was compared with values of permeability in real world fractured aquifers. De Fillipis et al. (2016) presented a study of saline intrusion in a karstic coastal aquifer in the Taranto area of Northern Italy. The lowest hydraulic conductivity values (of the order of 10^{-4} m/sec) were calculated inland and along the extremely western coast, while the central and eastern coastline part of the aquifer had a hydraulic conductivity of 0.1 m/sec, or approximately 9.07×10^{-9} m^2. In an investigation of SWI in a fractured aquifer in Crete, Greece (Steiakakis et al., 2016) a permeability of 1.35×10^{-10} m^2 was reported for the limestone portion of the hydrological system. A comparable permeability value was identified for the fracture-karst aquifer in Zhoushuizi district of Dalian City in northern China (Zhao et al., 2016). Xu and Hu (2017) introduced a numerical model for simulating seawater intrusion to a coastal karst aquifer with a conduit system. A porous medium permeability equal to 2.4×10^{-9} m^2 was derived from previous field scale studies (Loper et al., 2005; Kincaid and Werner, 2008; Xu et al., 2016) of the Floridan aquifer in

the Woodville Karst Plain, in Florida (USA). Finally, a study of the coastal carbonate aquifer in western Cuba (Hernandez-Diaz et al., 2019) reported an aquifer permeability equal to 1.1×10^{-9} m^2. The real-world fractured aquifer permeabilities values presented in this paragraph, have a difference of less than an order of magnitude from the permeability of the utilised glass bead medium. This validates the current laboratory setup as an acceptable approximation of saltwater dynamics in fractured hydrological systems.

The sandbox fracture permeability was determined via sensitivity analysis, conducted using the numerical model presented in the next session. The fractures (steel mesh tube) were approximately 100 times more permeable than the surrounding porous medium (glass beads). This permeability ratio is in agreement with fieldwork investigations of fractured aquifers. McAllister et al. (2018) in their study of the Seaford and Lewes Nodular Chalk formations in the UK, reported intrinsic fracture permeabilities 100 to 150 times larger than the rest of the aquifer. Similarly, Xu and Hu (2017) identified a conduit network that was 250 times more permeable than the porous medium of the Floridian karst aquifer.

In the initial stage of each experiment, freshwater occupied the whole aquifer. Saltwater was introduced to the system by applying a hydraulic head difference dH = 6 mm between the two side chambers of the laboratory apparatus. After the stabilization of the saline wedge, a new phase of saline intrusion was initiated by modifying the hydraulic head difference from 6mm to 4mm. In the final part of the experiments saltwater retreat was generated by applying a steeper hydraulic gradient (dH= 4 mm – 5 mm) in the aquifer. The resulting hydraulic gradients were similar to those documented for various real world aquifers (Attanayake and Sholley, 2007; Ferguson and Gleesson, 2012). The total measurement time varied between 160 and 180 minutes in the seven investigated cases, depending on the time needed for the saline wedge to stabilize after changing the head difference. During the experiment, water in the right cylinder was monitored using a YSI Professional Plus Instrument (Pro Plus) water quality meter. The salinity values for all six experiments, obtained at five-minute intervals, demonstrated minimum variation (Figure S1 of the supplementary material) indicating that water salinity in the right chamber did not reduce due to the outflow of freshwater through the porous medium.

The automated image analysis algorithms introduced by Robinson et al. (2015) and Etsias et al. (2020 a and b) were utilized to successfully post-process the acquired experimental images. An Artificial Neural Network (ANN) with a single hidden layer, consisting of 10 neurons, was employed to recreate saltwater concentration fields from the corresponding Light Intensity (LI) values of the laboratory test images (Figure 3). Two variables were calculated utilizing image processing to quantify the effect of fractures on aquifer saline intrusion: TL and WMZ. TL was deemed equivalent to the horizontal distance between the saltwater boundary of the laboratory aquifer and the point where the 50 % saltwater concentration isoline intersected with the bottom of the aquifer, while WMZ equated to the average vertical distance between the 25 % and 75 % saltwater concentration isolines. The automated calculation of these variables was described in detail by Robinson et al. 2015.

3. Numerical modelling

The experimental saltwater flow fields were simulated utilizing a 2-dimensional, saturated-unsaturated, variable-density groundwater flow model in SUTRA (Voss and Provost, 2010), where the fractures were modelled discretely as 2-dimensional elements (DFM 2D/2D). Permeability and porosity were equal to 1.83×10^{-9} m^2 and 0.385, respectively. Fracture permeability was determined, via sensitivity analysis, being 100 times larger than that of the matrix, while the porosity of fractures was set equal to 1. Since the size of the mesh tubes was approximately 0.8 cm, and turbulent flow is

not relevant inside fractures with a diameter of less than 1 cm (White et al., 2019), Darcian flow was considered in both media (matrix and fracture). The highest velocity inside the fracture (0.0337 m/sec) was recorded in the horizontal-long case for an applied hydraulic gradient of DH = 6mm. This results in a low Reynolds number, equal to 256.3, clearly indicating laminar flow inside the mesh tube. The x-z two-dimensional flow model, with dimensions of 0.38 m × 0.134 m, was discretized with a finite element mesh with quadrangular elements of a size of 1.22×10^{-3} m. The element size complied with the Peclet number criterion (Voss and Souza 1987), while the applied dispersivity values were within the range introduced by Abarca and Clement (2009). Unsaturated flow was simulated utilizing the van Genuchten equation (van Genuchten, 1980). Van Genuchten parameters were determined according to values measured in laboratory testing for glass beads of comparable size (Benson et al. 2014, Sweijan et al. 2017). A hydrostatic freshwater (C = 0 %) boundary condition was applied on the left boundary while a hydrostatic saltwater (C = 100 %) boundary condition was implemented on the right boundary of the aquifer. A necessary step towards the successful numerical recreation of the laboratory data was the precise identification of the position of the fracture in each test case. This was achieved through image analysis of the original experimental figures and the subsequent distribution of all the corresponding elements of the numerical model in either the matrix or the fracture medium. The simulation time for each test case was similar to the equivalent experimental duration, while the time-step was equal to 1 sec. Model parameters are listed in Table 1. A comparison between experimental and numerical results is presented in Figures 3 and 4.

Table 1: Summary of the discrete fracture matrix model parameters

Input parameters	Values
Domain length (m)	0.38
Domain height (m)	0.134
Element size (m)	1.22×10^{-3}
Freshwater density (kg/m^3)	1000
Saltwater density (kg/m^3)	1025
Freshwater head (m)	0.134
Saltwater head (m)	0.128 -0.13
Porous medium (matrix)	
Permeability (m^2)	1.83×10^{-9}
Porosity	0.385
Fracture	
Permeability (m^2)	1.83×10^{-7}
Porosity	1
Longitudinal dispersivity (m)	10^{-3}
Transverse dispersivity (m)	3.75×10^{-5}
Van Genuchten parameters	
α (1/Pa)	8.45×10^{-4}
n	4.5
Time step (sec)	1
Simulation time (min)	
Simulating exp. aquifers	50-70
Sensitivity Analysis	80

The conclusions about the impact of fractures on SWI, derived from experimental observations, were investigated further through a rigorous sensitivity analysis using the aforementioned numerical model. In total four different model setups were created, in three of them the fractures' orientation

was horizontal while in the fourth one it was vertical. This sensitivity analysis expanded the study's findings on the effect of the fractures' position, orientation and length on aquifer saltwater dynamics.

4. Results and discussion

4.1 Experimental results

The experimental saltwater flow fields that were generated inside the sandbox setup, by a hydraulic head difference between the left and right aquifer boundaries equal to dH = 4mm, are presented in Figure 3. The saline concentration fields derived by experimental image analysis and numerical modelling (SUTRA) are displayed alongside them. Alongside saltwater concentration, SUTRA calculates the flow velocity vectors at each individual element. The flow streamlines plotted on top of the numerical saltwater concentration fields in the third column of Figure 3 were generated by feeding the numerical flow velocities into the streamslice.m built-in MATLAB equation. This is a standard function developed by Mathworks and included in the MATLAB R2018a release. The results demonstrated that the position, size and orientation of discontinuities have a significant impact on the extent of saltwater intrusion, as well as the shape of saline wedges in fractured systems. The toe length has been a long established metric of the extend of saline intrusion. Nevertheless, in cases like the horizontal-long aquifer (Figure 3b), even though the observed TL value was relatively big, the actual volume of the aquifer occupied by saltwater was disproportionally small. On that account, the uniquely shaped freshwater - saltwater interfaces, generated by the presence of high permeability fractures, required the use of a supplementary variable to help quantify and assess the successful study of SWI. This novel variable, now termed as the saline volume fraction, corresponded to the fraction of the porous medium in which saltwater concentration was higher than 90%. It was calculated with high accuracy by the aforementioned image analysis algorithms and has been utilized for the first time in this study.

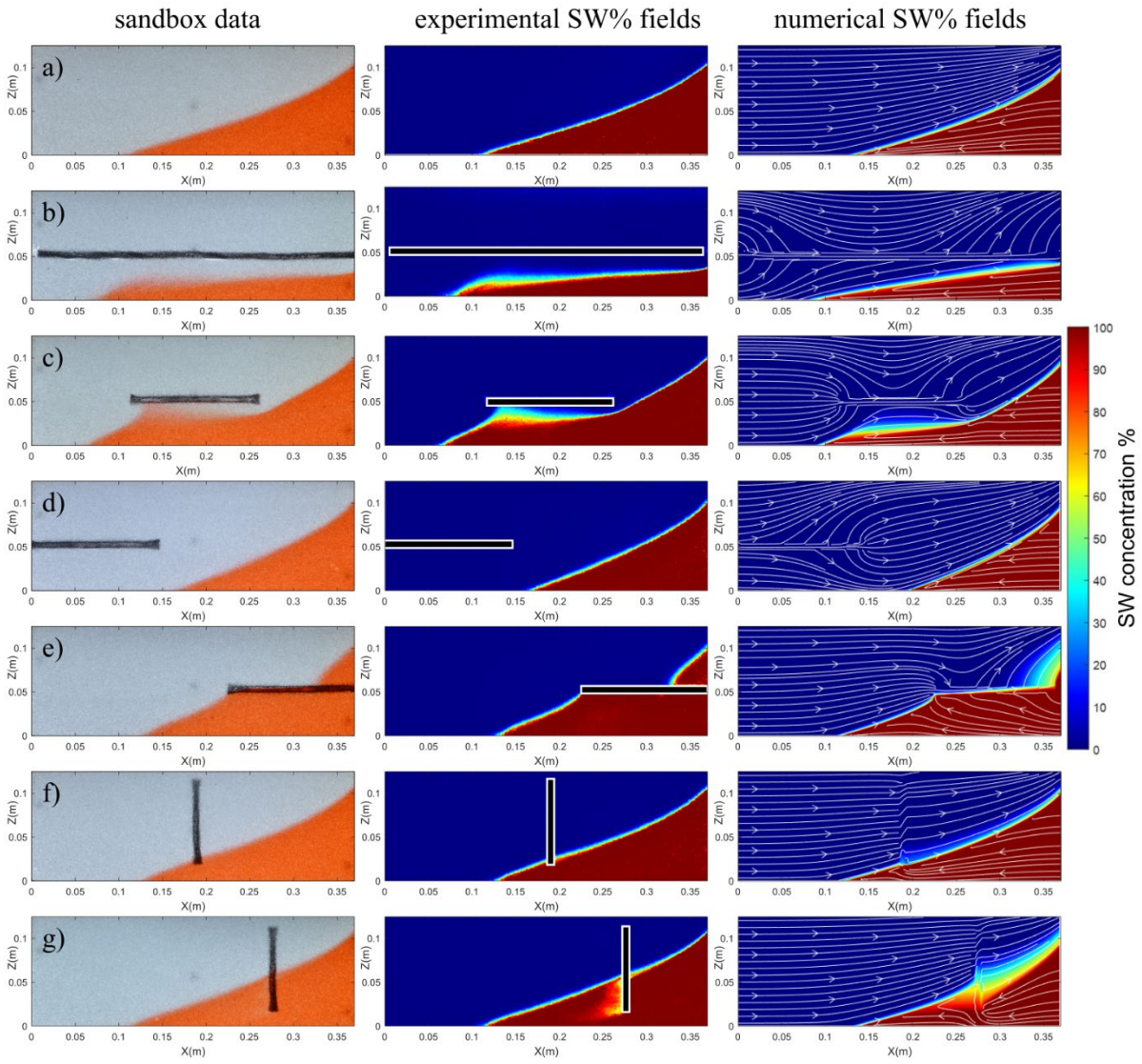

Figure 3: Photos of laboratory induced saline intrusion alongside experimental and numerical saltwater concentration fields in the seven investigated aquifers. From top to bottom the investigated cases are a) homogeneous aquifer, b) horizontal-long, c) horizontal-middle, d) horizontal-left, e) horizontal-right, f) vertical-middle and g) vertical-right fractured aquifers.

The numerical model successfully recreated the laboratory results for all three distinct intrusion and retreat (dH = 6 mm – 4 mm – 5 mm) experimental phases, for all the tested cases (Figure 4). In all cases, there is excellent temporal agreement between the measured values of TL and those obtained from the numerical simulations. Furthermore, it proved that using a dual-porosity model to simulate the sandbox data was a valid choice, and that this model can be safely employed to both interpret the physical mechanisms affecting SWI in the specific laboratory aquifers, as well as to further expand any conclusions derived from their study. As expected, the experimental TL was negatively correlated with the applied hydraulic gradient. The difference between the three steady state TL values (Table 2) was more significant in the horizontal-long aquifer, where $\Delta TL_{6\text{-}4mm}$ = +25.95 cm and $\Delta TL_{4\text{-}5mm}$ = -11.83 cm, while it was minimum for the horizontal-right case, $\Delta TL_{6\text{-}4mm}$ = +8.7 cm and $\Delta TL_{4\text{-}5mm}$ = -5.78 cm. This demonstrated that, the size and position of the discontinuity can significantly affect the impact of hydraulic head difference on the extend of saline intrusion. Every change in the hydraulic gradient was followed by an initial, rapid adjustment of the toe length, which subsequently stabilized. The time to

reach steady state in each intrusion and retreat phase did not vary much between the six investigated fractured cases. This is in agreement with the laboratory findings of Robinson et al. (2016) indicating that this time depends solely on the permeability of the porous medium, which was the same in all laboratory setups.

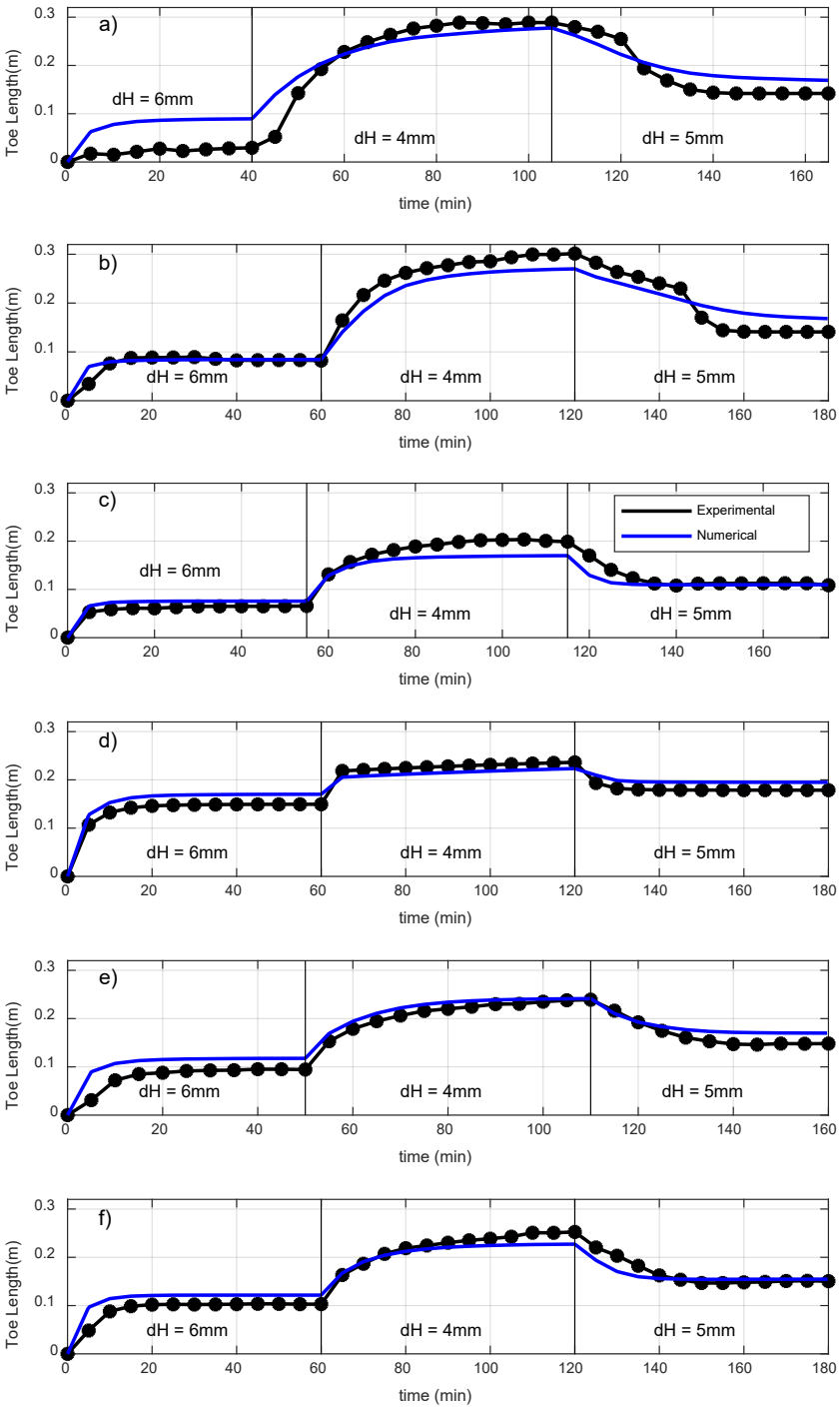

Figure 4: Experimental and numerical transient toe length values of the a) horizontal-long, b) horizontal-middle, c) horizontal-left, d) horizontal-right, e) vertical-middle and f) vertical-right fractured aquifers

Table 2: Steady-state toe length values of the seven investigated laboratory aquifers, and the corresponding relative change in TL generated during the experimental intrusion (dH = 6 – 4 mm) and retreat (dH = 4 – 5 mm) phases

Aquifer TL (cm)	dH = 6 mm	dH =4 mm	dH = 5 mm	$\Delta TL\%_{6\text{-}4mm}$	$\Delta TL\%_{4\text{-}5mm}$
homogeneous	12.10	25.38	14.29	+109.75	-43.70
horizontal-long	2.94	28.89	17.06	+882.65	-40.95
horizontal-middle	8.22	30.14	14.82	+266.67	-50.83
horizontal-left	6.57	20.34	10.87	+209.59	-46.56
horizontal-right	14.94	23.64	17.86	+58.23	-24.45
vertical-middle	9.44	23.91	14.82	+153.28	-38.02
vertical-right	10.30	25.25	15.06	+145.15	-40.36

The three variables outlining the effect of fractures on saline intrusion: TL, WMZ and the percentage of aquifer saline volume, were quantified. Their values were benchmarked against the SWI characteristics in the homogeneous laboratory aquifer with the same permeability and porosity values (Table 3). It was established that, in comparison to the homogeneous case, TL was significantly longer for the horizontal-long and horizontal-middle aquifers, by 13.8 % and 18.7 % respectively, while it was about 19.9 % and 6.9 % shorter for the horizontal-left and horizontal-right cases. No quantifiable deviation in the TL values was observed for the systems with vertical fracture orientation. The mixing zone in all the fractured cases was wider than that in the homogeneous aquifer. In particular, for the horizontal-long, horizontal-middle and vertical-right systems, WMZ was more than double the width of the benchmark case (220 % ~ 285 % of the homogeneous WMZ), while for the remaining three fractured aquifers it was between 21 % and 52 % wider. The total volume fraction of the aquifer occupied by the saline wedge was significantly smaller for the horizontal-long and horizontal-left cases, being equal to just 49.1 % and 78.2 % of the equivalent saline volume fraction in the homogeneous case. In the remaining fractured aquifers saline volume fraction did not deviate significantly, ranging between 93.5 % and 105.9 % of the benchmark case.

Table 3: Comparison between the experimental values of toe length, width of the mixing zone and percentage of saline volume of the six investigated fractured aquifers and the ones of the equivalent homogeneous aquifer

	Fractured / Homogeneous (%)		
Fractured aquifer	TL	WMZ	Saline Volume
horizontal-long	113.82	220.74	49.11
horizontal-middle	118.76	285.01	105.98
horizontal-left	80.15	120.92	78.27
horizontal-right	93.12	151.93	93.47
vertical-middle	97.22	150.66	97.89
vertical-right	99.51	244.95	100.88

To assess the interpretation of the acquired experimental data and to outline the basic physical mechanisms behind the impact of fractures on SWI dynamics, the velocity vector fields of the seven investigated hydraulic systems were recreated using SUTRA (Figure 5). In Figure 5, the magnitude of

flow velocities is expressed with varying colour instead of varying vector lengths, as it is commonly demonstrated (e.g. Abdoulhalik and Ahmed 2017a). This was deliberately chosen by the authors to assess velocity visualization, since freshwater, both inside the fractures and the porous medium, flows with a velocity that is at least an order of magnitude greater than that of the saltwater. Figure 5a depicts the typical flow velocity distribution occurring during SWI on a homogeneous aquifer. This constitutes a well-documented mechanism; the less dense freshwater overtops saltwater and outflows from the upper right area of the quasi 2-dimensional system. Flow velocity is considerably higher for the freshwater than the saltwater and its magnitude peaks around the outflow zone. In the simulated aquifer depicted in Figure 5b (horizontal-long), two distinct zones of higher velocity were observed at the entrance and exit of the long fracture. The presence of the fracture caused the majority of freshwater mass transport to occur through it, while at the same time limiting the flow of freshwater in the rest of the system, as depicted by the smaller velocity (dark blue) vectors around the central mesh cylinder. This absence of freshwater at the lower part of the aquifer resulted in longer saline intrusion near the aquifer's bottom. Saltwater did not intrude over the fracture, accounting for the relatively small portion of the aquifer being occupied by the saline wedge (Table 3). The horizontal - middle aquifer (Figure 5c) constituted a hydraulic system similar to the horizontal – long one, with the exception of a shorter fracture. Yet again, two distinct zones of higher freshwater velocity were documented at the fracture's edges. The upward movement of freshwater towards the fracture once more augmented SWI. Freshwater outflow from the fracture's right edge contributed to the saline wedge's distinct shape. Lu et al. (2013) indicated that according to conservation of mass, separation of flow streamlines along the freshwater - saltwater interface results in the widening of the mixing zone. This separation, observed in the areas directly underneath the horizontal discontinuities (Figures 3b and 3c), alongside the small difference between the flow velocities of the two liquids at the same zone, attributed for the distinctively wider mixing zone in these two systems. The saline volume fraction of the horizontal - middle system was equal to 105.9 % of the saline volume in the benchmark homogeneous case.

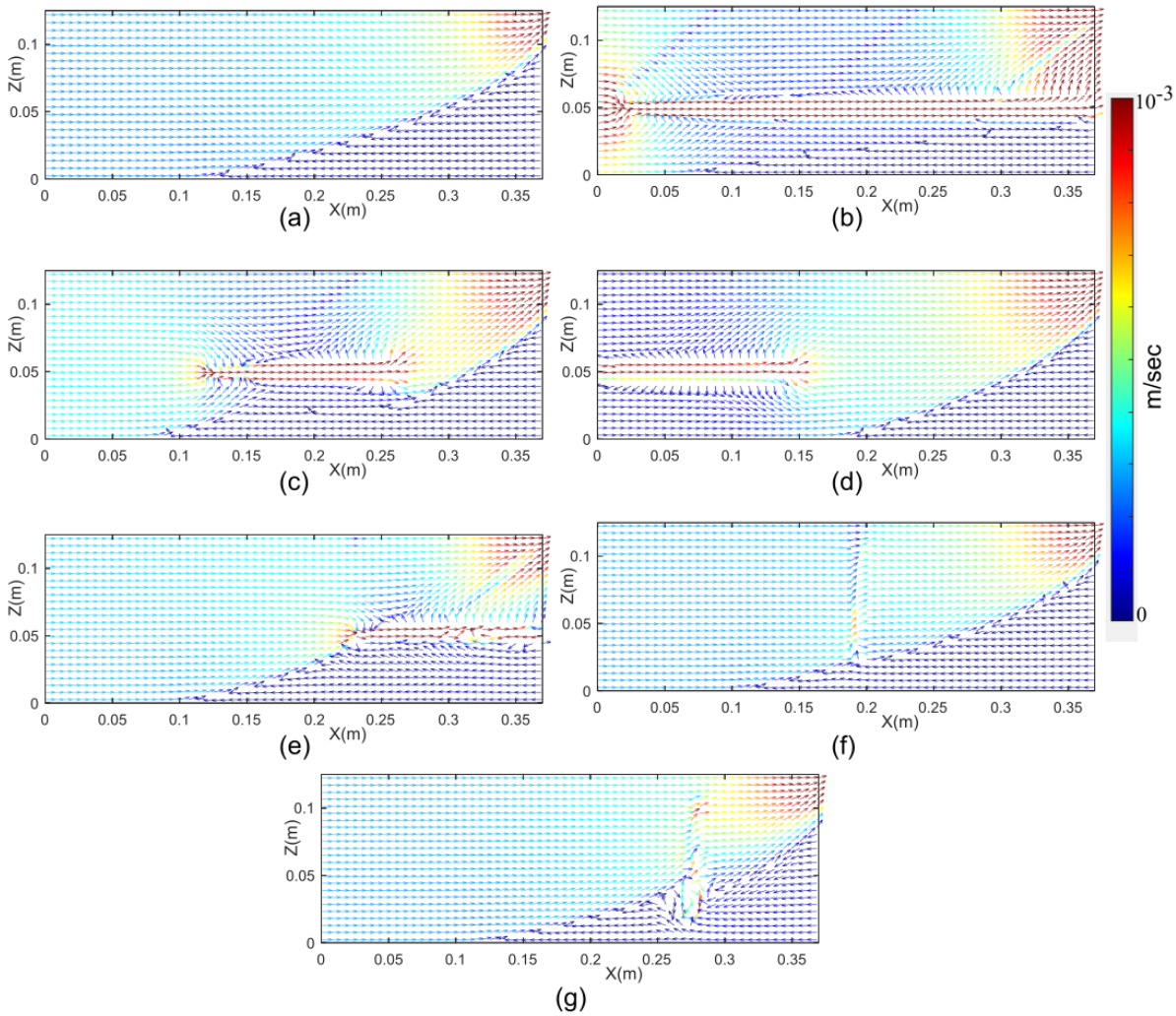

Figure 5: Flow velocity vector fields, generated by a hydraulic head difference of 4 mm for the a) horizontal-long, b) horizontal-middle, c) horizontal-left, d) horizontal-right, e) vertical-middle, f) vertical-right fractured and the g) homogeneous aquifer

In the horizontal-left (Figure 5d) and horizontal-right (Figure 5e) laboratory aquifers the same fracture was placed at diametrically opposite positions, resulting in two distinct saltwater concentration distributions. In the horizontal-left system the majority of freshwater inflow into the porous medium occurred through the fracture. Two distinct velocity zones were observed in the aquifer: a low velocity one directly above and below the fracture, and a relatively large area of high velocity vector fields at the fracture's right edge. The presence of faster moving freshwater at the centre of the system resulted in the seaward suppression of saltwater, while the saline wedge's shape was comparable to that of the homogeneous case albeit with a smaller TL (Table 2). In the horizontal-right aquifer, where the fracture was in direct proximity with the saltwater boundary, the majority of the water outflowed from this discontinuity as depicted by the relatively lower velocities at the upper right edge of the system. These two zones of water outflow caused by the position of the cylindrical mesh resulted in a uniquely shaped saltwater wedge. Yet again, the wider mixing zone directly above the fracture should be attributed to the separation of streamlines. The total saline volume in this system was equivalent to 93.5 % of the saltwater volume in the homogeneous case.

In the experimental aquifers with vertically oriented fractures, the observed steady-state saltwater wedges were similar in shape and size to the one recreated in the homogeneous aquifer. In particular, for the vertical-middle and vertical-right systems, TL equalled to 97.2 % and 99.5 % of the benchmark case, while saline volume corresponded to 97.9 % and 100.9 % of the saltwater in the homogeneous aquifer. The vector fields presented in Figures 5f and 5g indicate that the impact of these fractures on the total distribution of flow was limited. In the vertical-middle case, where the saline wedge never reached the hollow mesh cylinder, the fracture caused a slight variation in the direction and magnitude of the velocities in its interior that had limited effect on the rest of the system. On the other hand, in the vertical-right aquifer where the saltwater wedge extended beyond the fracture's position, the velocity vector fields inside the mesh structure indicate the intensification of the water recirculation that normally occurs inside the saline wedges. This increased water recirculation justifies the widening of the mixing zone around the fracture, documented in both Figures 3g and Table 3. Although this phenomenon was previously reported in purely numerical investigations (Sebben et al., 2015), it was identified on a laboratory scale for the first time in this study.

Overall, the experimental data derived from the six fractured aquifers allowed identification of some preliminary trends concerning the impact that individual fractures have on SWI characteristics. It was established that depending on its length and position, horizontally oriented fractures can either augment or suppress saltwater intrusion, while significantly affecting WMZ and the total volume of intruding saltwater. On the other hand, vertical fractures contributed to the widening of the mixing zone, but had a limited impact on the actual length and shape of the intruding wedge. These findings were further expanded in the following section, using a series of sensitivity analysis scenarios.

4.2 Sensitivity analysis

The sensitivity analysis presented here comprises four distinct scenarios, each one examining SWI in five numerical aquifers. The utilized model parameters were the same as those used in simulating the experimental saltwater concentration fields (Table 1). Saline intrusion was initiated by applying a hydraulic head difference of 4 mm, while a total run time of 80 minutes ensured that all systems reached quasi steady-state. A fifth set of numerical simulations, where different values of hydraulic gradients were applied to the system, supplemented the findings of the first sensitivity analysis scenario. Unlike the numerical models presented in the previous section in which the fractures' shape and position were determined using image analysis, all fissures present in this investigation had an idealized rectangular shape. In order to assess comparison between experimental data and those derived from the sensitivity analysis, the saltwater concentration fields presented in this section include only the part of the aquifer that it is visible in the laboratory sandbox setup. When determining the depth of discontinuities, the whole height of the numerical aquifer was taken into account, instead of just the part included in the viewing chamber. As a result, discontinuities in this section was placed approximately two centimetres higher than the fractures in the laboratory test cases of the previous section.

4.2.1 Horizontal position of horizontally oriented fractures

In the first sensitivity analysis setup, the impact of position (x) of horizontal fractures on SWI dynamics was investigated. To do so, five aquifers containing a single horizontal fracture with dimensions of 15.4 cm × 0.85 cm (126 × 7 elements) were generated. The fractures were placed at the middle of the aquifers' depth. On the horizontal direction, they were either placed adjacent to the system's vertical boundaries (Figures 6a.i and 6a.v), at a distance of 5 cm from them (Figures 6a.ii and 6a.iv) or exactly at the aquifer's centre (Figure 6a.iii). As seen in Figure 6, the closer the fracture was to the freshwater boundary, the more it contributed to the suppression of saline intrusion, while the closer its proximity

413 to the seaward edge, the longer the length of the intruding wedge was (Figure 6b). This is in agreement
414 with the experimental observations presented in section 4.1. The positive correlation between TL and
415 fracture position (x) was disrupted in the case where the fracture was in contact to the sea (right
416 boundary). The adjacency of the high permeability fracture with the saline boundary created two
417 zones of water outflow from the porous medium, significantly altering the underlying flow and mass
418 transport mechanisms. Moreover, the slightly smaller fracture depth in the numerical aquifers of this
419 section is responsible for the difference between the saltwater concentration field depicted in Figure
420 6a.v and that in Figure 3e. Similarly, the mixing zone is widened when the velocity difference between
421 the two fluids is smaller (Figure 6c). This occurred in the low velocity zones underlying the fractures
422 (Figure 6a). The impact of these zones was greater with increasing proximity to the freshwater –
423 saltwater interface. This resulted in a mixing zone, that was three times wider in the aquifer depicted
424 in Figure 6a.iv than in the system illustrated in Figure 6a.i. Finally, a positive correlation was
425 established between the fracture's proximity with the sea boundary and the total volume of the
426 intruding saltwater (Figure 6d), leading to a maximum difference of up to 13 % between the saline
427 volume fraction values of the five test cases.

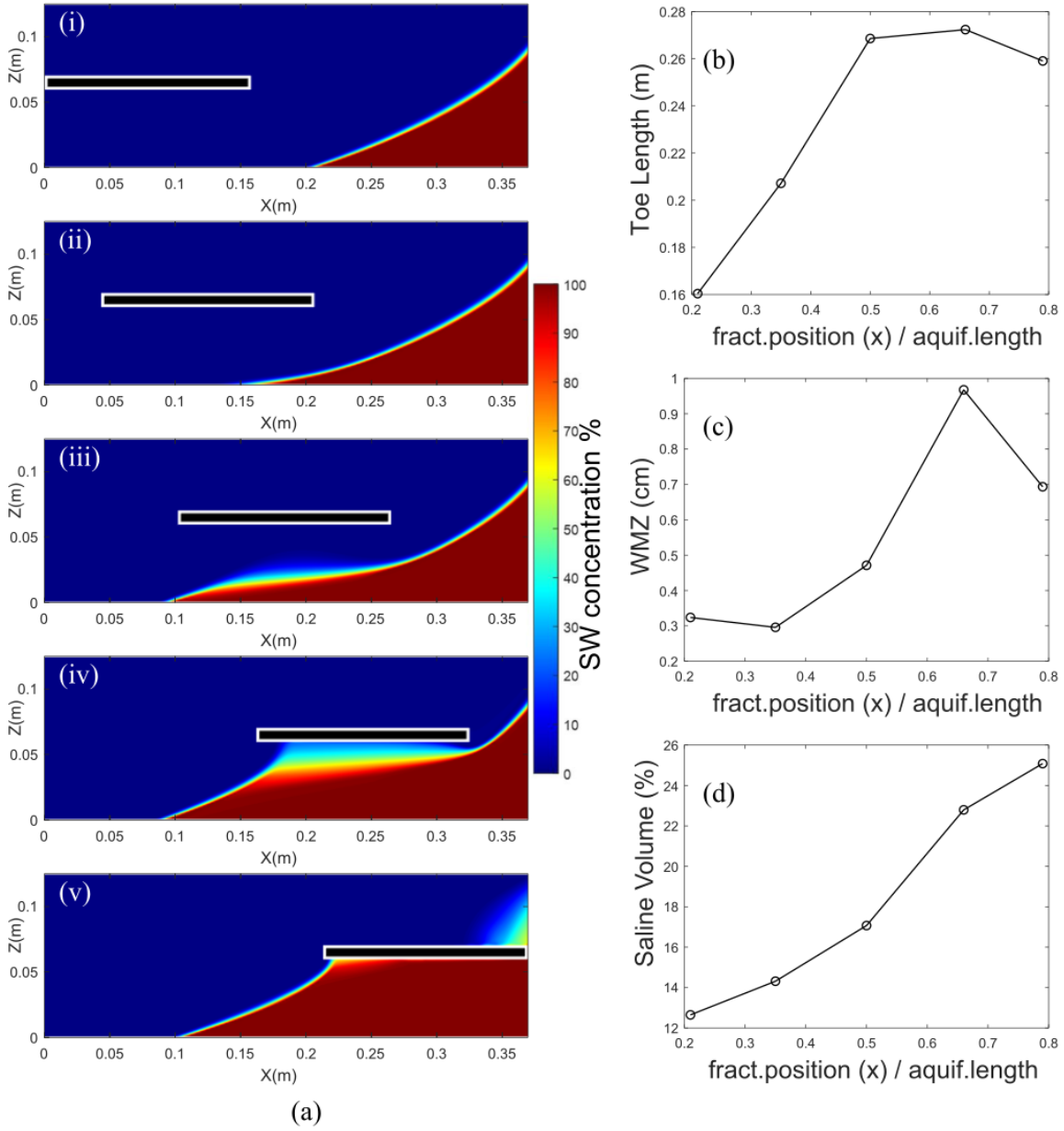

Figure 6: Simulated a) SW concentration fields alongside their corresponding values of b) toe length, c) width of mixing zone and d) percentage of saline volume, demonstrating the impact of position (x) of a horizontal fracture on aquifer SWI

In order to identify the main factors determining whether the presence of a discontinuity results in less or more extended saline intrusion, a supplemental set of numerical simulations were conducted. In total four aquifers were investigated: the centrally fractured case, presented in Figure 6a.iii; two fractured aquifers, with a discontinuity at 7.5 cm from the aquifer's left and right boundary; and a homogeneous system with similar porous medium characteristics. SWI was initiated in these aquifers by applying seven distinct values of hydraulic head difference (dH = 4 mm, 4.5 mm, 5 mm, 5.5 mm, 6 mm, 6.5 mm and 7 mm). The generated steady-state TL values are presented in Figure 7. The numerical results indicated that, depending on the applied hydraulic gradient, the same fracture can lead to an intruding wedge that is either longer or shorter than the one in the equivalent homogeneous case. The critical head difference, at which TL was the same for both the fractured and

the homogeneous aquifer, was different for each case. Its value was equal to dH = 4.17 mm, dH = 5.97 mm and dH = 4.88 mm for the systems fractured on their left side, right side, and in the middle respectively. The equivalent TL values for these hydraulic gradients were equal to 22.3 cm, 12 cm and 17.1 cm. When compared to the horizontal position (fracture's centre from the seaward boundary) of the discontinuity in each system, x_{left} = 23.1 m, x_{right} = 13.1 m and x_{middle} = 18.1 m, a clear linear relationship between the critical TL value and the discontinuity's position arises. Summarising, the findings of the numerical investigation proved that the impact of horizontal fractures on the extent of intrusion depends on both their position and the applied hydraulic gradient. In cases where the fracture's distance from the seaward boundary was greater than the saline toe length in the equivalent homogeneous system, for the same hydraulic gradient, the presence of the discontinuity limited the extent of intrusion, while in cases where this distance was smaller it augmented it. This conclusion has potentially significant implications for the effective management of real-world fractured aquifers, since the projected sea-level rise could alter their hydraulic gradient beyond its critical value, thus leading to a significant and unexpected increase in the extent of saltwater intrusion.

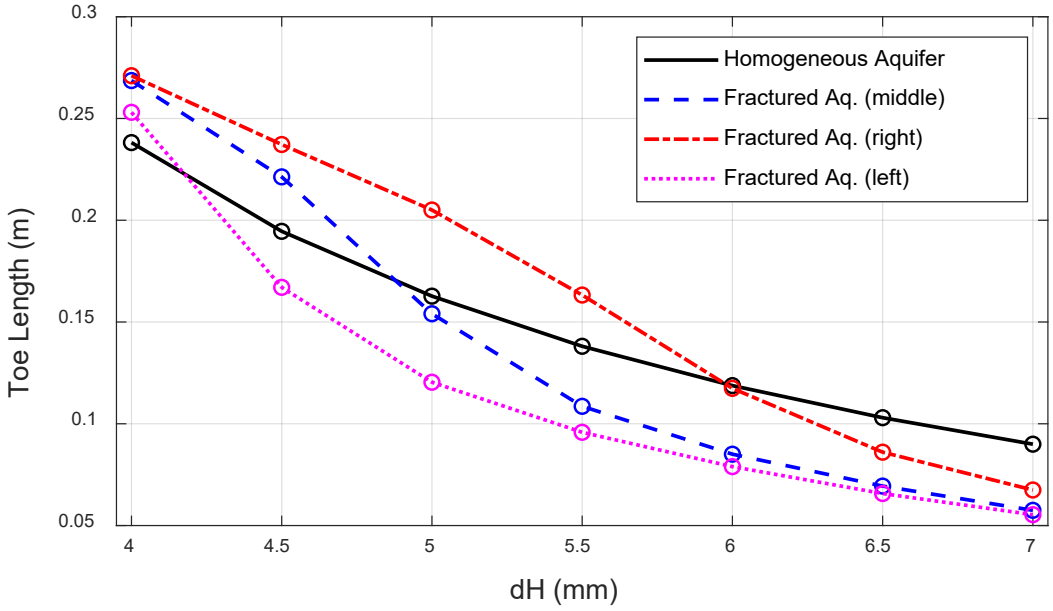

Figure 7: Values of saltwater toe length generated by the application of seven distinct hydraulic head difference values (dH = 4 mm – 7 mm) in one homogeneous (black) and three heterogeneous aquifers, containing a single horizontal fracture at their right (red) and left (purple) side, and their middle (blue) respectively

4.2.2 Depth location of horizontally oriented fractures

Five numerical fractured aquifers were utilized to quantify the effect that the depth below the surface (z) of horizontal discontinuities has on saltwater intrusion. A fracture with the same dimensions to those described in the previous section was located at a depth form the system's surface equal to 1/6, 1/3, 1/2, 2/3 and 5/6 of the total aquifer width. As seen in Figure 8, the impact of fractures on the saltwater – freshwater interface became greater the closer the discontinuity was to the impermeable lower boundary. For the majority of the test cases, the TL was positively correlated to the fracture's distance from the aquifer's free surface (Figure 8b). Nevertheless, TL variation between the different aquifers of this setup was much more limited. The shortest TL (Figure 8a.i) equalled to 94.2 % of the longest TL case (Figure 8ai.v), translating into a difference of less than 2 cm. In comparison, maximum toe length difference in the previous sensitivity analysis scenario was approximately 11 cm, or a

472 minimum TL value corresponding to just 58.9 % of the maximum TL. Similar to the previous set of
473 numerical investigations, this trend did not apply to the last test aquifer (Figure 8a.v), where the length
474 of the intruding wedge was shorter than the previous cases. The physical mechanism described for
475 the experimental horizontal – middle aquifer (section 4.1) also applied to these numerical aquifers as
476 well. However, the fracture's impact proved greater with decreasing distance from the interface of
477 the two liquids. The correlation between fracture depth (z) and WMZ was similar to that reported for
478 the toe length (Figure 8c), while the total volume of intruding saltwater was negatively correlated to
479 the fracture's distance from the system's upper boundary (Figure 8d) resulting in an absolute
480 difference of up to 5 % between the investigated aquifers. For all the scenario's test cases, saline
481 volume constituted a fraction (72.3 % - 97.3 %) of the volume in the equivalent homogeneous case.
482 The current analysis demonstrated that even though the vertical position of a discontinuity has a
483 limited effect on the final length of the intruding wedge, it can significantly influence the extent of
484 intrusion at the upper parts of an aquifer. This could constitute a significant finding in the successful
485 management of real-life fractured systems, where SWI in the upper aquifer region could significantly
486 damage human activities such as farming (Alam et al., 2017).

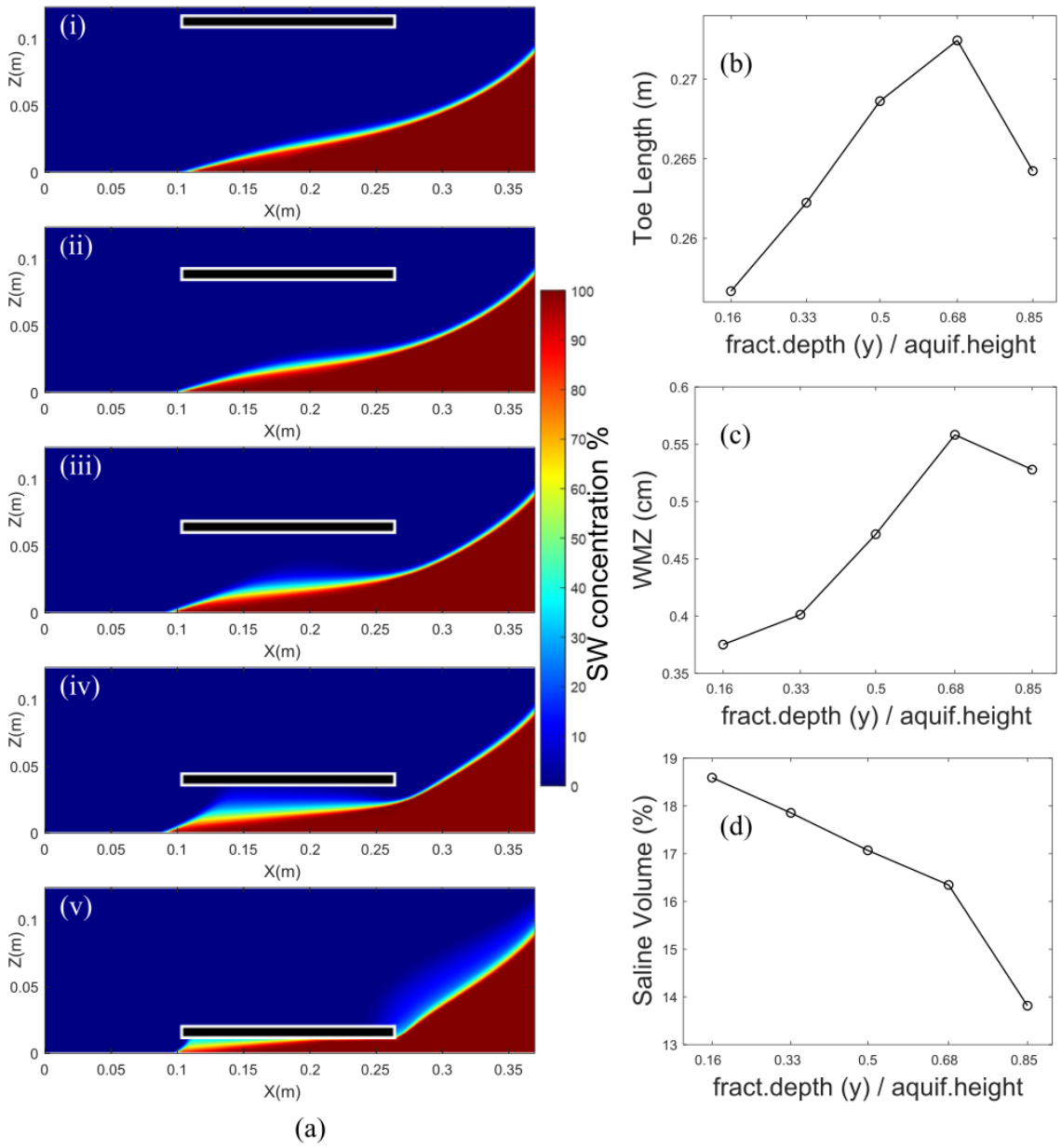

Figure 8: Simulated a) SW concentration fields alongside their corresponding values of b) toe length, c) width of mixing zone and d) percentage of saline volume, demonstrating the impact of position (z) of a horizontal fracture on aquifer SWI

4.2.3 Length of horizontally oriented fractures

The effect of fracture length on saline intrusion dynamics was studied on the third sensitivity analysis setup. Aquifers with a single horizontal fracture of a width of 0.85 cm and a varying length equal to 1/6, 1/3, 1/2and 2/3 of the total aquifer length, as well as an aquifer with a fracture spanning from one aquifer edge to the other, were tested. With the exception of the last case, the numerical results indicated a positive relationship between fracture length and length of intrusion (Figure 9b). The longer the discontinuities, the larger the zones of lower freshwater velocity underneath them, leading to more space occupied by saltwater. The maximum difference between the TL values generated in this scenario was less than 5 cm. Both WMZ (Figure 9c) and the total volume of the saline water (Figure 9d) were affected by the fracture length in a similar way. The unique shape of the intruding wedge in

the last investigated aquifer (Figure 9a.v), comparable to the interface shape of the horizontal-long (Figure 3b) experimental system, indicated a fundamentally different flow mechanism. This could be attributed to the fact that the bulk of the mass transport inside the system occurred exclusively through its discontinuity, contributing to the limited impact of dispersion effects.

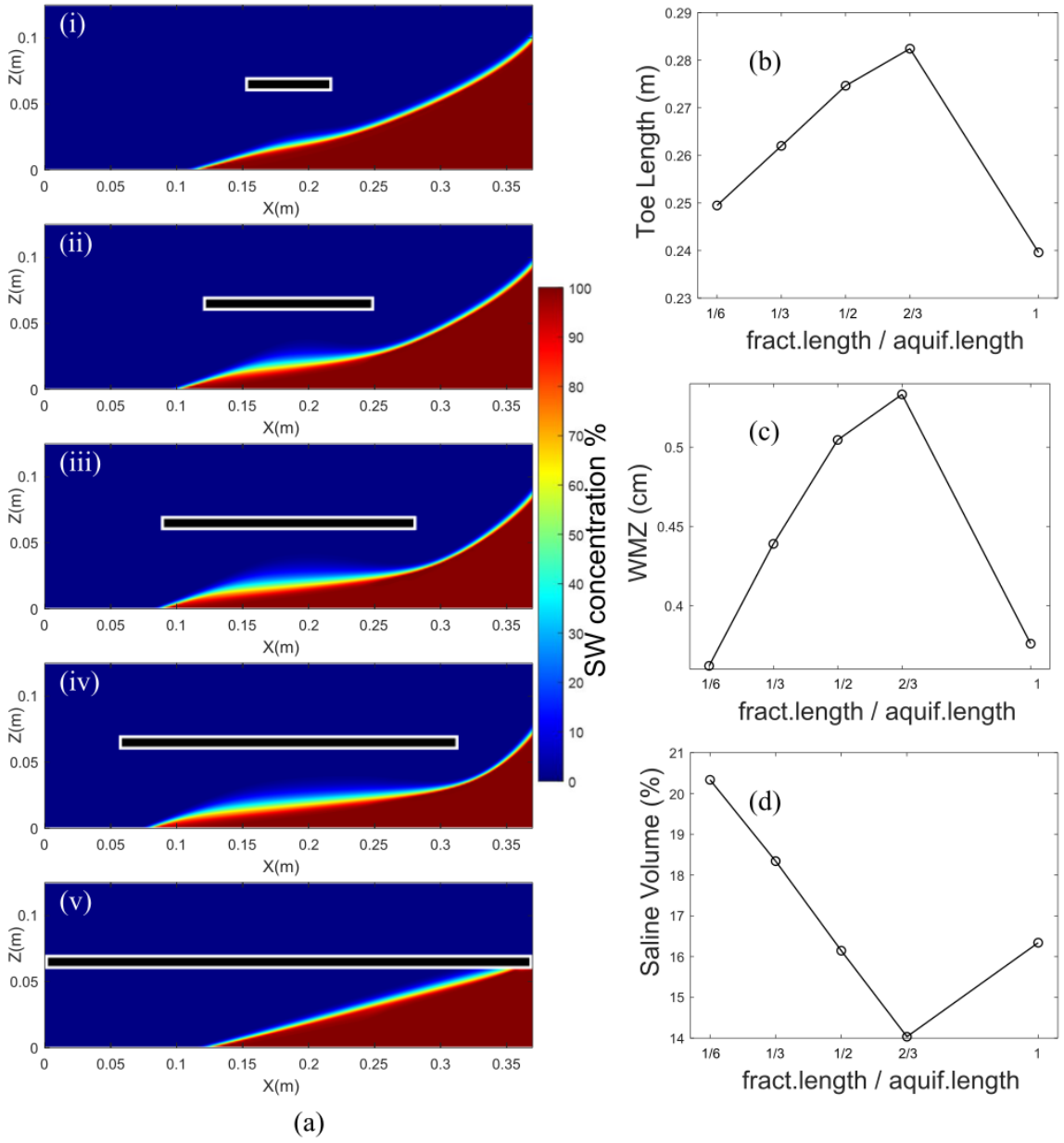

Figure 9: Simulated a) SW concentration fields alongside their corresponding values of b) toe length, c) width of mixing zone and d) percentage of saline volume, demonstrating the impact of a horizontal fracture's length on aquifer SWI

4.2.4 Horizontal position of vertically oriented fractures

The final sensitivity analysis setup investigated the influence that the position (x) of vertical discontinuities has on aquifer saline intrusion. Five numerical aquifers with fractures of dimensions 0.85 cm × 11.8 cm placed at different distances from the system's side boundaries were the basis of this study (Figure 10a). It was shown that the impact of the discontinuities' position on the steady-

state length of intrusion was relatively limited, causing a TL variation of less than 12 % between the five tested cases (Figure 10b). On the other hand, the width of the mixing zone was significantly affected by the fractures' location. In aquifers where the intruding saline wedge incorporated the discontinuities, WMZ widened by up to 12 cm in comparison to the cases where the fractures were fully covered by freshwater (Figure 10c). This constituted an increase of approximately 400 %. The correlation between the position of vertical discontinuities and the width of mixing zone is in agreement with the relationship derived by the experimental measurements (section 4.1) as well as the numerical findings of Sebben et al. (2015). The impact of flow recirculation effects inside the discontinuity was more severe on its downstream than its upstream area, i.e. right of the fracture in the investigated numerical setup. This justifies why the increase in WMZ was larger in the numerical aquifer depicted on Figure 10a.iv, where the fracture was approximately at the middle of the intruding wedge. Finally, since no significant alteration of the traditional wedge shape was observed in any aquifer, the trend in the total volume of intruding saltwater was comparable to that of the TL values (Figure 10d). The deviation of saline volume fraction was 5% or less between the investigated fractured systems.

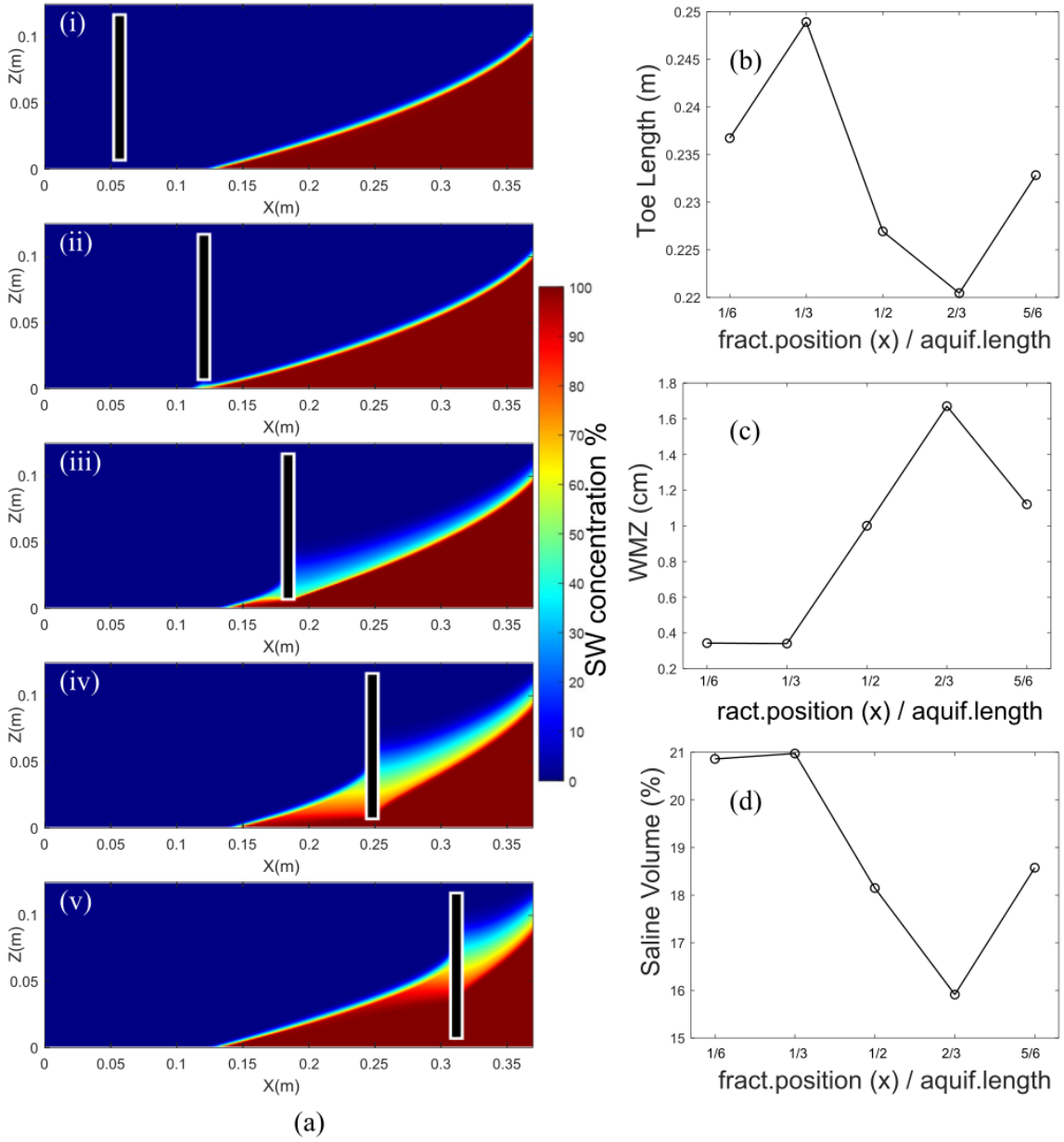

Figure 10: Simulated a) SW concentration fields alongside their corresponding values of b) toe length, c) width of mixing zone and d) percentage of saline volume, demonstrating the impact of position (x) of a vertical fracture on aquifer SWI

The sensitivity analysis results presented here further expanded the findings derived in section 4.1. Horizontally oriented fractures were proven to have a significant impact in both TL, WMZ and the total volume of intruding saltwater. In cases where horizontal discontinuities were present further toward the freshwater reservoir, they tended to limit the extent of saline intrusion, while the opposite occurred as the fractures were closer to the sea. Even though TL values were relatively unaffected by the depth in which such fractures were located, their vertical position determined the height up to which saltwater would intrude. To that effect, the fractures acted as high permeability barriers confining SWI to the lower aquifer levels. This indicated that the impact of horizontal fractures on saline intrusion dynamics was greater with increasing length. Finally, vertical fractures widened the

freshwater - saltwater mixing zone, with their effect proving greater when positioned in the middle of the intruding wedges.

5. Conclusions

Saltwater intrusion in fractured unconfined coastal aquifers was studied on a laboratory scale for the first time in the current paper. Saline intrusion was initiated in a thin sandbox setup by applying three distinct hydraulic gradients. A total of six fractured systems, with discontinuities of different size and orientation, were tested alongside one homogeneous aquifer with similar porous medium attributes. Automated image analysis enabled the recreation of saltwater concentration fields as well as the precise calculation of three SWI characteristics: the length of intruding wedge, the width of the mixing zone and the aquifer volume fraction occupied by saltwater. The experimental results were successfully simulated using a dual porosity model in SUTRA. This model was subsequently employed in conducting a detailed sensitivity analysis to validate and expand the findings derived from the laboratory data.

It was established that the presence of fractures significantly impacts all three saltwater intrusion variables. The impact of four specific fracture attributes was investigated, the fracture's horizontal and vertical position, its length and its orientation. The following conclusions can be drawn:

- In cases where horizontal discontinuities were present closer to the aquifer's saline boundary, the extent of saltwater intrusion was generally bigger, while in systems where the fractures were further away from the sea, the saline wedge was reduced. Rigorous sensitivity analysis revealed that the extent to which a discontinuity affects the toe length of the intruding wedge depends on two variables: its horizontal position and the hydraulic gradient applied in the system. A critical hydraulic head difference was identified as the defining factor behind the discontinuity's impact on saline intrusion for each specific fractured system. For hydraulic gradients steeper than this head difference, the fracture's presence limits the intrusion, while for milder gradients it intensifies it.
- The vertical distance of horizontal fractures from the aquifer's free surface was positively correlated to the generated saline wedge length and width of mixing zone, while negatively correlated to the percentage of saltwater volume. Discontinuities acted similar to high permeability barriers, confining the saline wedge in the aquifer's lower level.
- The longer the discontinuities were, the more pronounced their effect was on all three saltwater intrusion characteristics.
- Vertical fractures had a limited effect on the length of intrusion and the total aquifer fraction occupied by saltwater. On the other hand, they had a significant impact on the width of the mixing zone, resulting in its increase by a factor of up to four, under the scenarios investigated. This effect was more intense in cases where the fractures were located in the middle of the saline wedges.
- Whenever the discontinuities were in contact to the aquifer's freshwater or saltwater side boundaries, the generated concentration fields deviated significantly from the rest of the cases, indicating a critical alteration of the underlying flow mechanisms.

This study outlined the effects of individual fractures on the dynamics of saltwater intrusion in coastal aquifers. The two-dimensional nature of the laboratory setup, alongside the simplified geometry of the investigated fractures and the homogeneous nature of the surrounding porous medium, enabled the identification of the fundamental physical flow mechanisms generated by the presence of high permeability - high porosity discontinuities without the uncertainty that usually accompanies the study of SWI on field scale investigations. Even though derived for idealized conditions, the findings

of this study could be of significant importance for the effective management of real-world fractured aquifers. Moreover, the precise laboratory data presented in this study may be employed to benchmark numerical models studying saline intrusion in fractured media. Future work could expand the conclusions of this study by investigating more complex configurations of fractures with varying size and orientation, as well as different boundary conditions and porous medium characteristics.

Acknowledgements

This work was funded by EPSRC Standard Research (Grant No. EP/R019258/1).

References

Abarca, E., Clement, T.P., 2009. A novel approach for characterizing the mixing zone of a saltwater wedge. Geophys. Res. Lett. 36 (6), L06402.

Abdelgawad, A. M., Abdoulhalik, A., Ahmed, A. A., Moutari, S., & Hamill, G. (2018). Transient Investigation of the Critical Abstraction Rates in Coastal Aquifers: Numerical and Experimental Study. Water Resources Management, 32(11), 3563-3577. doi:10.1007/s11269-018-1988-3

Abdoulhalik, A., & Ahmed, A. A. (2017a). The effectiveness of cutoff walls to control saltwater intrusion in multi-layered coastal aquifers: Experimental and numerical study. Journal of Environmental Management, 199, 62-73. doi: 10.1016/j.jenvman.2017.05.040

Abdoulhalik, A., & Ahmed, A. A. (2017b). How does layered heterogeneity affect the ability of subsurface dams to clean up coastal aquifers contaminated with seawater intrusion? Journal of Hydrology, 553, 708–721. doi: 10.1016/j.jhydrol.2017.08.044

Arfib, B., & Charlier, J.-B. (2016). Insights into saline intrusion and freshwater resources in coastal karstic aquifers using a lumped Rainfall–Discharge–Salinity model (the Port-Miou brackish spring, SE France). Journal of Hydrology, 540, 148–161. doi: 10.1016/j.jhydrol.2016.06.010

Arfib, B., & Marsily, G. D. (2004). Modeling the salinity of an inland coastal brackish karstic spring with a conduit-matrix model. Water Resources Research, 40(11). doi: 10.1029/2004wr003147

Alam, M. Z., Carpenter-Boggs, L., Mitra, S., Haque, M. M., Halsey, J., Rokonuzzaman, M., Moniruzzaman, M. (2017). Effect of Salinity Intrusion on Food Crops, Livestock, and Fish Species at Kalapara Coastal Belt in Bangladesh. Journal of Food Quality, 2017, 1–23. doi: 10.1155/2017/2045157

Allen, D.M., Liteanu, E., & Mackie, D.C. (2003). Geologic controls on the occurrence of saltwater intrusion in heterogeneous and fractured island aquifers, southwestern British Columbia, Canada. Proceedings of 2nd International Conference on Saltwater Intrusion in Coastal Aquifers – Monitoring, Modeling, and Management, Mérida, México (2003)

Angot, P., Boyer, F., & Hubert, F. (2009). Asymptotic and numerical modelling of flows in fractured porous media. ESAIM: M2AN, 43(2), 239-275. doi: 10.1051/m2an/2008052

Armanuos, A. M., Ibrahim, M. G., Mahmod, W. E., Takemura, J., & Yoshimura, C. (2019). Analysing the Combined Effect of Barrier Wall and Freshwater Injection Countermeasures on Controlling Saltwater Intrusion in Unconfined Coastal Aquifer Systems. Water Resources Management, 33(4), 1265–1280. doi: 10.1007/s11269-019-2184-9

Arthur, J. D., Wood, H. A. R., Baker, A. E., Cichon, J. R., & Raines, G. L. (2007). Development and Implementation of a Bayesian-based Aquifer Vulnerability Assessment in Florida. Natural Resources Research, 16(2), 93–107. doi: 10.1007/s11053-007-9038-5

Attanayake, P., & Sholley, M. (2007). Evaluation of the hydraulic gradient at an island for low-level nuclear waste disposal. *IAHS publication*, *312*, 237.

Bakalowicz, M., Hakim, M. E., & El-Hajj, A. (2007). Karst groundwater resources in the countries of eastern Mediterranean: the example of Lebanon. Environmental Geology, 54(3), 597–604. doi: 10.1007/s00254-007-0854-z

Benson, C. H., Chiang, I., Chalermyanont, T., & Sawangsuriya, A. (2014). Estimating van Genuchten Parameters α and n for Clean Sands from Particle Size Distribution Data. From Soil Behavior Fundamentals to Innovations in Geotechnical Engineering. doi: 10.1061/9780784413265.033

Berre, I., Doster, F., & Keilegavlen, E. (2018). Flow in Fractured Porous Media: A Review of Conceptual Models and Discretization Approaches. Transport in Porous Media, 130(1), 215–236. doi: 10.1007/s11242-018-1171-6

Blessent, D., Jørgensen, P. R., & Therrien, R. (2013). Comparing Discrete Fracture and Continuum Models to Predict Contaminant Transport in Fractured Porous Media. Groundwater, 52(1), 84–95. doi: 10.1111/gwat.12032

Chen, Z., Auler, A. S., Bakalowicz, M., Drew, D., Griger, F., Hartmann, J., … Goldscheider, N. (2017). The World Karst Aquifer Mapping project: concept, mapping procedure and map of Europe. Hydrogeology Journal, 25(3), 771–785. doi: 10.1007/s10040-016-1519-3

Custodio, E. (2009). Coastal aquifers of Europe: an overview. Hydrogeology Journal, 18(1), 269–280. doi: 10.1007/s10040-009-0496-1

Dose, E. J., Stoeckl, L., Houben, G. J., Vacher, H., Vassolo, S., Dietrich, J., & Himmelsbach, T. (2014). Experiments and modeling of freshwater lenses in layered aquifers: Steady state interface geometry. Journal of Hydrology, 509, 621–630. doi: 10.1016/j.jhydrol.2013.10.010

Dokou, Z., & Karatzas, G. P. (2012). Saltwater intrusion estimation in a karstified coastal system using density-dependent modelling and comparison with the sharp-interface approach. Hydrological Sciences Journal, 57(5), 985–999. doi: 10.1080/02626667.2012.690070

Etsias, G., Hamill, G., Benner, E., Aguila, J.F., McDonnell, M., Flynn & R., Ahmed, A.A. (2020 a) Optimizing Laboratory Investigations of Saline Intrusion by Incorporating Machine Learning Techniques. Water 2020, 12, 2996. doi: 10.3390/w12112996

Etsias, G., Hamill, G., Benner, E., Aguila, J.F., McDonnell, & M., Flynn (2020 b) The effect of colour Depth and image resolution on laboratory scale study of aquifer saltwater intrusion. Proceedings of CERAI, 27 - 28 August 2020, Cork, Ireland.

Fahs, H., Hayek, M., Fahs, M., & Younes, A. (2014). An efficient numerical model for hydrodynamic parameterization in 2D fractured dual-porosity media. Advances in Water Resources, 63, 179–193. doi: 10.1016/j.advwatres.2013.11.008

Faulkner, J., Hu, B. X., Kish, S., & Hua, F. (2009). Laboratory analog and numerical study of groundwater flow and solute transport in a karst aquifer with conduit and matrix domains. Journal of Contaminant Hydrology, 110(1-2), 34–44. doi: 10.1016/j.jconhyd.2009.08.004

Feo, A., Zanini, A., Petrella, E., Hernàndez-Diaz, R., & Celico, F. (2019). Analysis of the Saltwater Wedge in a Coastal Karst Aquifer with a Double Conduit Network, Numerical Simulations and Sensitivity Analysis. Water, 11(11), 2311. doi: 10.3390/w11112311

Ferguson, G., & Gleeson, T. (2012). Vulnerability of coastal aquifers to groundwater use and climate change. *Nature Climate Change*, *2*(5), 342-345.

Filippis, G. D., Foglia, L., Giudici, M., Mehl, S., Margiotta, S., & Negri, S. L. (2016). Seawater intrusion in karstic, coastal aquifers: Current challenges and future scenarios in the Taranto area (southern Italy). Science of The Total Environment, 573, 1340–1351. doi: 10.1016/j.scitotenv.2016.07.005

Flemisch, B., Berre, I., Boon, W., Fumagalli, A., Schwenck, N., Scotti, A., . . . Tatomir, A. (2018). Benchmarks for single-phase flow in fractured porous media. Advances in Water Resources, 111, 239-258. doi: 10.1016/j.advwatres.2017.10.036

Ford D, Williams P (2007) Karst hydrogeology and geomorphology. Wiley, Chichester, UK

Genuchten, M. T. V. (1980). A Closed-form Equation for Predicting the Hydraulic Conductivity of Unsaturated Soils. Soil Science Society of America Journal, 44(5), 892–898. doi: 10.2136/sssaj1980.03615995004400050002x

Giudici, M., Margiotta, S., Mazzone, F., Negri, S., & Vassena, C. (2012). Modelling hydrostratigraphy and groundwater flow of a fractured and karst aquifer in a Mediterranean basin (Salento peninsula, southeastern Italy). Environmental Earth Sciences, 67(7), 1891–1907. doi: 10.1007/s12665-012-1631-1

Hernàndez-Diaz, R., Petrella, E., Bucci, A., Naclerio, G., Feo, A., Sferra, G., . . . Celico, F. (2019). Integrating Hydrogeological and Microbiological Data and Modelling to Characterize the Hydraulic Features and Behaviour of Coastal Carbonate Aquifers: A Case in Western Cuba. Water, 11(10), 1989. doi:10.3390/w11101989.

Hirthe, E. M., & Graf, T. (2015). Fracture network optimization for simulating 2D variable-density flow and transport. Advances in Water Resources, 83, 364–375. doi: 10.1016/j.advwatres.2015.07.001

Houben, G. J., Stoeckl, L., Mariner, K. E., & Choudhury, A. S. (2018). The influence of heterogeneity on coastal groundwater flow - physical and numerical modeling of fringing reefs, dykes and structured conductivity fields. Advances in Water Resources, 113, 155–166. doi: 10.1016/j.advwatres.2017.11.024

Khadra, W. M., & Stuyfzand, P. J. (2018). Simulation of saltwater intrusion in a poorly karstified coastal aquifer in Lebanon (Eastern Mediterranean). Hydrogeology Journal, 26(6), 1839–1856. doi: 10.1007/s10040-018-1752-z

Kincaid, T. R., & Werner, C. L. (2008). Conduit Flow Paths and Conduit/Matrix Interactions Defined by Quantitative Groundwater Tracing in the Floridan Aquifer. In Sinkholes and the Engineering and Environmental Impacts of Karst (2008) (pp. 288-302).

Konz, M., Ackerer, P., Meier, E., Huggenberger, P., Zechner, E., & Gechter, D. (2008). On the measurement of solute concentrations in 2-D flow tank experiments. Hydrology and Earth System Sciences, 12(3), 727–738. doi: 10.5194/hess-12-727-2008

Konz, M., Younes, A., Ackerer, P., Fahs, M., Huggenberger, P., & Zechner, E. (2009). Variable-density flow in heterogeneous porous media — Laboratory experiments and numerical simulations. Journal of Contaminant Hydrology, 108(3-4), 168-175. doi:10.1016/j.jconhyd.2009.07.005

Koohbor, B., Fahs, M., Ataie-Ashtiani, B., Belfort, B., Simmons, C. T., & Younes, A. (2019). Uncertainty analysis for seawater intrusion in fractured coastal aquifers: Effects of fracture location, aperture, density and hydrodynamic parameters. Journal of Hydrology, 571, 159–177. doi: 10.1016/j.jhydrol.2019.01.052

Koohbor, B., Fahs, M., Hoteit, H., Doummar, J., Younes, A., & Belfort, B. (2020). An advanced discrete fracture model for variably saturated flow in fractured porous media. Advances in Water Resources, 140, 103602. doi: 10.1016/j.advwatres.2020.103602

Kreyns, P., Geng, X., & Michael, H. A. (2020). The influence of connected heterogeneity on groundwater flow and salinity distributions in coastal volcanic aquifers. Journal of Hydrology, 586, 124863. doi: 10.1016/j.jhydrol.2020.124863

Larsbo, M., & Jarvis, N. (2005). Simulating Solute Transport in a Structured Field Soil: Uncertainty in Parameter Identification and Predictions. Journal of Environmental Quality, 34(2), 621–634. doi: 10.2134/jeq2005.0621

Li, G., 2004. Laboratory Simulation of Solute Transport and Retention in a Karst Aquifer, Program in Geophysical Fluid Dynamics, Florida State University.

Li, F.L., Chen, X.-Q., Liu, C.-H., Lian, Y.-Q., & He, L. (2018). Laboratory tests and numerical simulations on the impact of subsurface barriers to saltwater intrusion. Natural Hazards, 91(3), 1223–1235. doi: 10.1007/s11069-018-3176-4

Lim, J.-W., Lee, E., Moon, H. S., & Lee, K.-K. (2013). Integrated investigation of seawater intrusion around oil storage caverns in a coastal fractured aquifer using hydrogeochemical and isotopic data. Journal of Hydrology, 486, 202–210. doi: 10.1016/j.jhydrol.2013.01.023

Liu, Y., Mao, X., Chen, J., & Barry, D. A. (2013). Influence of a coarse interlayer on seawater intrusion and contaminant migration in coastal aquifers. Hydrological Processes, 28(20), 5162–5175. doi: 10.1002/hyp.10002

Loper, D. E., Werner, C. L., Chicken, E., Davies, G., & Kincaid, T. (2005). Coastal carbonate aquifer sensitivity to tides. Eos, Transactions American Geophysical Union, 86(39), 353. doi:10.1029/2005eo390001

Lu, C., Chen, Y., Zhang, C., & Luo, J. (2013). Steady-state freshwater–seawater mixing zone in stratified coastal aquifers. Journal of Hydrology, 505, 24–34. doi: 10.1016/j.jhydrol.2013.09.017

Macallister, D., Jackson, M. D., Butler, A. P., & Vinogradov, J. (2018). Remote Detection of Saline Intrusion in a Coastal Aquifer Using Borehole Measurements of Self-Potential. Water Resources Research, 54(3), 1669–1687. doi: 10.1002/2017wr021034

Martin, V., Jaffré, J., Roberts, J.E. (2005). Modeling fractures and barriers as interfaces for flow in porous media. SIAM J. Sci. Comput. 26(5), 1667–1691. doi:10.1137/s1064827503429363

Masciopinto, C. (2006). Simulation of coastal groundwater remediation: the case of Nardò fractured aquifer in Southern Italy. Environmental Modelling & Software, 21(1), 85–97. doi: 10.1016/j.envsoft.2004.09.028

745 Mehdizadeh, S. S., Werner, A. D., Vafaie, F., & Badaruddin, S. (2014). Vertical leakage in sharp-interface
746 seawater intrusion models of layered coastal aquifers. Journal of Hydrology, 519, 1097–1107.
747 doi: 10.1016/j.jhydrol.2014.08.027

748 Montiel, D., Dimova, N., Andreo, B., Prieto, J., Garcia-Orellana, J., & Rodellas, V. (2017). Assessing
749 Submarine Groundwater Discharge (Sgd) In Highly Heterogeneous Coastal Karst Aquifers:
750 Challenges and Solutions. doi: 10.1130/abs/2017cd-292389

751 Mozafari, B., Fahs, M., Ataie-Ashtiani, B., Simmons, C. T., & Younes R. (2018). On the use of COMSOL
752 Multiphysics for seawater intrusion in fractured coastal aquifers. Proceedings of 25th Salt
753 Water Intrusion Meeting, 17-22 June 2018, Gdansk Poland.

754 Nocchi, M., & Salleolini, M. (2013). A 3D density-dependent model for assessment and optimization
755 of water management policy in a coastal carbonate aquifer exploited for water supply and fish
756 farming. Journal of Hydrology, 492, 200–218. doi: 10.1016/j.jhydrol.2013.03.048

757 Papadopoulou, M. P., Varouchakis, E. A., & Karatzas, G. P. (2009). Terrain Discontinuity Effects in the
758 Regional Flow of a Complex Karstified Aquifer. Environmental Modeling & Assessment, 15(5),
759 319–328. doi: 10.1007/s10666-009-9207-5

760 Perriquet, M., Leonardi, V., Henry, T., & Jourde, H. (2014). Saltwater wedge variation in a non-
761 anthropogenic coastal karst aquifer influenced by a strong tidal range (Burren, Ireland).
762 Journal of Hydrology, 519, 2350–2365. doi: 10.1016/j.jhydrol.2014.10.006

763 Quinn, J. J., Tomasko, D., & Kuiper, J. A. (2006). Modeling complex flow in a karst aquifer. Sedimentary
764 Geology, 184(3-4), 343–351. doi: 10.1016/j.sedgeo.2005.11.009

765 Ren, F., Ma, G., Wang, Y., Li, T., & Zhu, H. (2017). Unified pipe network method for simulation of water
766 flow in fractured porous rock. Journal of Hydrology, 547, 80–96. doi:
767 10.1016/j.jhydrol.2017.01.044

768 Robinson, G., Ahmed, A. A., & Hamill, G. (2016). Experimental saltwater intrusion in coastal aquifers
769 using automated image analysis: Applications to homogeneous aquifers. Journal of Hydrology,
770 538, 304–313. doi: 10.1016/j.jhydrol.2016.04.017

771 Robinson, G., Hamill, G., & Ahmed, A. A. (2015). Automated image analysis for experimental
772 investigations of salt water intrusion in coastal aquifers. Journal of Hydrology, 530, 350–360.
773 doi: 10.1016/j.jhydrol.2015.09.046

774 Romanazzi, A., Gentile, F., & Polemio, M. (2015). Modelling and management of a Mediterranean
775 karstic coastal aquifer under the effects of seawater intrusion and climate change.
776 Environmental Earth Sciences, 74(1), 115–128. doi: 10.1007/s12665-015-4423-6

777 Samardzioska, T., & Popov, V. (2005). Numerical comparison of the equivalent continuum, non-
778 homogeneous and dual porosity models for flow and transport in fractured porous media.
779 Advances in Water Resources, 28(3), 235–255. doi: 10.1016/j.advwatres.2004.11.002

780 Scanlon, B. R., Mace, R. E., Barrett, M. E., & Smith, B. (2003). Can we simulate regional groundwater
781 flow in a karst system using equivalent porous media models? Case study, Barton Springs
782 Edwards aquifer, USA. Journal of Hydrology, 276(1-4), 137–158. doi: 10.1016/s0022-
783 1694(03)00064-7

784 Sebben, M. L., Werner, A. D., & Graf, T. (2015). Seawater intrusion in fractured coastal aquifers: A
785 preliminary numerical investigation using a fractured Henry problem. Advances in Water
786 Resources, 85, 93–108. doi: 10.1016/j.advwatres.2015.09.013

787 Sebben, M. L., & Werner, A. D. (2016). A modelling investigation of solute transport in permeable
788 porous media containing a discrete preferential flow feature. Advances in Water Resources,
789 94, 307–317. doi: 10.1016/j.advwatres.2016.05.022

790 Steiakakis, E., Vavadakis, D., Kritsotakis, M., Voudouris, K., & Anagnostopoulou, C. (2016). Drought
791 impacts on the fresh water potential of a karst aquifer in Crete, Greece. Environmental Earth
792 Sciences, 75(6). doi: 10.1007/s12665-016-5509-5

793 Sweijen, T., Aslannejad, H., & Hassanizadeh, S. M. (2017). Capillary pressure–saturation relationships
794 for porous granular materials: Pore morphology method vs. pore unit assembly method.
795 Advances in Water Resources, 107, 22–31. doi: 10.1016/j.advwatres.2017.06.00

796 Takahashi, M., Momii, K., & Luyun, R. (2018). Laboratory Scale Investigation of Dispersion Effects on
797 Saltwater Movement due to Cutoff Wall Installation. E3S Web of Conferences, 54, 00038. doi:
798 10.1051/e3sconf/20185400038

799 Vithanage, M., Engesgaard, P., Jensen, K., Illangasekare, T., & Obeysekera, J. (2012). Laboratory
800 investigations of the effects of geologic heterogeneity on groundwater salinization and flush-
801 out times from a tsunami-like event. Journal of Contaminant Hydrology, 136-137, 10–24. doi:
802 10.1016/j.jconhyd.2012.05.001Van Genuchten, M.T., 1980. A closed-form equation for
803 predicting the hydraulic conductivity

804 Voss, C., Provost, A., 2010. SUTRA—a Model for Saturated–unsaturated, Variabledensity Ground-
805 water Flow with Solute or Energy Transport, 2010. US Geological Survey Water-Resources
806 Investigations Report, 02-4231.

807 Voss, C. I., & Souza, W. R. (1987). Variable density flow and solute transport simulation of regional
808 aquifers containing a narrow freshwater-saltwater transition zone. Water Resources
809 Research, 23(10), 1851-1866.

810 White, W. B., Culver, D. C., & Pipan, T. (2019). Encyclopedia of caves. London: Elsevier, Academic Press.

811 Xu, Z., Bassett, S. W., Hu, B., & Dyer, S. B. (2016). Long distance seawater intrusion through a karst
812 conduit network in the Woodville Karst Plain, Florida. Scientific Reports, 6(1). doi:
813 10.1038/srep32235

814 Xu, Z., & Hu, B. X. (2017). Development of a discrete-continuum VDFST-CFP numerical model for
815 simulating seawater intrusion to a coastal karst aquifer with a conduit system. Water
816 Resources Research, 53(1), 688–711. doi: 10.1002/2016wr018758

817 Xu, Z., Hu, B. X., & Ye, M. (2018). Numerical modeling and sensitivity analysis of seawater intrusion in
818 a dual-permeability coastal karst aquifer with conduit networks. Hydrology and Earth System
819 Sciences, 22(1), 221–239. doi: 10.5194/hess-22-221-2018

820 Xu, Z., Hu, B. X., Xu, Z., & Wu, X. (2019). Simulating seawater intrusion in a complex coastal karst
821 aquifer using an improved variable-density flow and solute transport–conduit flow process
822 model. Hydrogeology Journal, 27(4), 1277–1289. doi: 10.1007/s10040-018-1903-2

823 Zhao, J., Lin, J., Wu, J., Yang, Y., & Wu, J. (2016). Numerical modeling of seawater intrusion in
824 Zhoushuizi district of Dalian City in northern China. Environmental Earth Sciences, 75(9). doi:
825 10.1007/s12665-016-5606-5

826